Abstract

In this research, the fluid-structure interaction in a recently developed membrane pump is analysed. The governing equations for the laminar flow and for the deformation of the membrane are solved with two separate codes, which are coupled with the quasi-Newton technique with an approximation for the inverse of the Jacobian from a least-squares model. After the description of the model and the solution techniques, a detailed analysis of the flow field, the deformation of the structure and the stress in the membrane is presented. An energetic analysis of the pump is performed, and the pump's efficiency is calculated.

Keywords: membrane pump, pumping of biological fluids, fluid-structure interaction, partitioned solution, interface quasi-Newton, mesh motion technique.

1 Introduction

The pumping of biological fluids, such as blood, or particle-laden fluids is a challenging problem. A first disadvantage of positive displacement pumps such as piston pumps or diaphragm pumps is that they provide a pulsating flow. Another drawback of these pumps is the presence of valves, which are fragile, expensive and need regular maintenance. Turbopumps can strike the biological fluid with their impellers or generate high shear stress which can damage the particles in the flow. Moreover, hard particles in the fluid can damage these pumps. In peristaltic pumps a rotor with a number of rollers compresses a flexible tube, forcing the fluid to move through the tube. However, the local high pressure areas in these pumps can be damaging for certain biological fluids.

The two pump types described below are based on other principles, making them better suited for the pumping of biological fluids. A first pump design ideally suited for

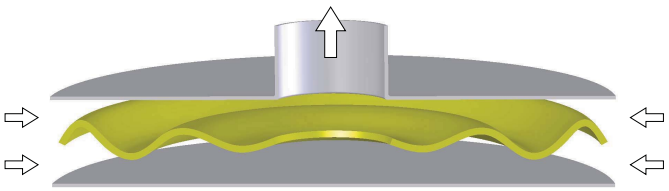

Figure 1: Illustration of a radial membrane pump.

biomedical applications is the multilayer impedance pump, inspired by the embryonic heart which achieves a unidirectional pumping prior to the valve formation [1]. The second pump type, analysed in this paper, is a recently developed membrane pump. The rigid casing of the pump consists of a hollow circular cylinder with a height that is smaller than its radius. This casing encloses a flexible, circular membrane with a hole at its centre. The membrane is held under tension by applying a force on the outer edge of the membrane. An electromagnet applies an oscillating motion parallel to the axis of the cylinder at the outer edge of the membrane. As a result, waves travel from the outer edge of the membrane towards its centre (see Figure 1). Energy is transferred from the membrane to the fluid during wave propagation. Hence, the fluid on both sides of the membrane is pumped from the inlet on the side of the cylinder to the outlet on the axis. If the excitation frequency is chosen high enough, the flow rate is more or less constant. By keeping an adequate distance between the membrane and the casing, damage to the particles in the flow is prevented. Modifying the amplitude of the excitation voltage makes it possible to generate pressure cycles that reproduce the heart beat cycles. This makes the pump suitable for biomedical applications in which extracorporeal blood circulation is involved.

In order to further improve the design of these pumps, deeper understanding of the fluid-structure interaction (FSI) in these pumps is required. In [2] the fluid-structure interaction in a multilayer impedance pump is investigated. The fluid-structure interaction in a radial membrane pump however had not yet been researched. The numerical simulation of such a multi-physics problem is challenging, especially as the interaction between the fluid and the structure is strong due to the flexibility of the structure and the comparable density of the fluid and the structure. The FSI problem is solved in a partitioned way, which means the flow and the structural equations are solved separately. This approach preserves software modularity and allows the flow equations and the structural equations to be solved with different techniques that are particularly suited to solve the respective equations. Besides a flow solver and a structural solver, also a coupling algorithm is required to take into account the interaction between flow and motion of the structure. In this research a quasi-Newton algorithm with an approximation for the inverse of the Jacobian (IQN-ILS) is used, which requires fewer coupling iterations per time step than dynamic relaxation techniques [3].

Apart from the interaction, another difficulty in the numerical simulation of these membrane pumps is the strongly deforming fluid domain, due to the large deformation

of the structure. An accurate calculation of the stress on the fluid-structure interface is obtained using the flow equations solved in the Arbitrary Lagrangian-Eulerian (ALE) formulation on a deforming mesh. However, with standard mesh motion techniques, it is impossible to maintain a valid, high-quality mesh throughout the simulations. This problem has been overcome by using an innovative combination of mesh motion corresponding to the solution of Laplace equations, mesh smoothing and remeshing.

2 Method

2.1 Physical model

In this research a two dimensional axisymmetric model of the pump was used. The dimensions of the pump are given in Table 1 and the geometry is shown in Figure 2. The fluid on both sides of the membrane is pumped from the outside of the cylinder towards its centre. The pumped fluid is water. The membrane is made of a silicone rubber. This material is inert, non-toxic and keeps its elasticity over a wide range of temperatures (173 K up to 573 K). The hyperelastic material behavior was described with the Van der Waals model. An electromagnet applies an oscillating motion parallel to the axis of the pump. We assumed that this electromagnet imposes a sinusoidal movement at the outer edge of the membrane. The sinusoidal excitation has a frequency of 50 Hz and an amplitude of 1 mm. A constant static pressure of 0 Pa is imposed at the outlet of the pump. The total pressure at the inlet is 0 Pa.

Parameter	Symbol	Value
Fluid domain radius	r_{pump}	46 mm
Fluid domain width	w_{pump}	11 mm
Internal radius of the structure	$r_{s,int}$	8 mm
External radius of the structure	$r_{s,ext}$	38 mm
Thickness of the structure	t_s	1 mm
Fluid density	ρ_f	998.2 kg/m^3
Fluid viscosity	μ_f	0.001003 kg/ms
Fluid specific heat	c_p	4182 J/kgK
Fluid thermal conductivity	K	0.6 W/mK
Structural density	ρ_s	1160 kg/m^3
Structural stiffness	E	1.4-2.3 N/mm^2
Excitation amplitude	A	1 mm
Excitation frequency	f	50 Hz

Table 1: Dimensions of the pump and the material properties.

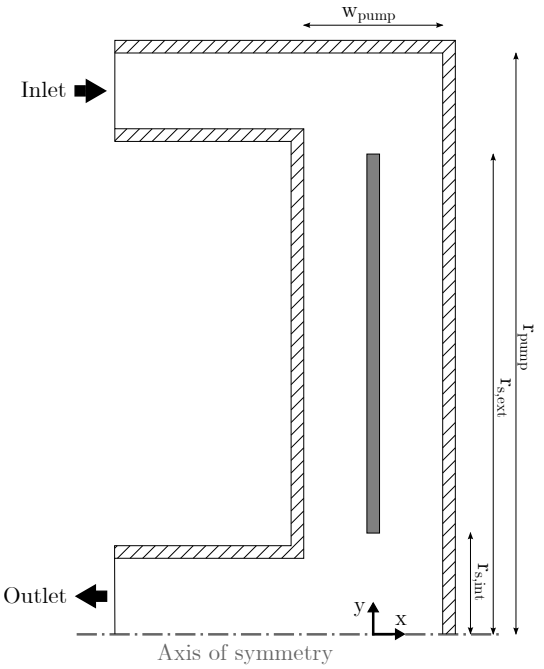

Figure 2: Geometry of the pump used in this research.

2.2 Mathematical Model

2.2.1 Flow equations

The equations that describe the unsteady flow of the Newtonian, incompressible, viscous fluid in the pump are the Navier-Stokes equations, given by

$$\nabla . \boldsymbol{v}_f = 0 \tag{1a}$$

$$\rho_f \frac{\partial \boldsymbol{v}_f}{\partial t} + \rho_f \nabla . (\boldsymbol{v}_f \boldsymbol{v}_f) + \nabla p = \rho_f \boldsymbol{f}_f + \nabla . \boldsymbol{\tau} \tag{1b}$$

$$\rho_f \frac{\partial E}{\partial t} + \rho_f \nabla . (H \boldsymbol{v}_f) = \rho_f \boldsymbol{f}_f . \boldsymbol{v}_f + \nabla . (\boldsymbol{\tau} . \boldsymbol{v}_f) - \nabla . (-K \nabla T) \tag{1c}$$

with $\boldsymbol{v}_f$ the flow velocity, ρ_f the fluid density, t the time, p the pressure. $\boldsymbol{f}_f$ represents the body forces per unit of mass on the fluid, $\boldsymbol{\tau}$ the viscous stress tensor, E the total energy of the flow (i.e. the sum of internal and kinetic energy), $H = E + p/\rho$ the total enthalpy, K the thermal conductivity and T the fluid temperature. The stress tensor $\boldsymbol{\sigma}_f$ is defined as

$$\boldsymbol{\sigma}_f = -p\boldsymbol{I} + \boldsymbol{\tau}, \tag{2}$$

with $\boldsymbol{I}$ the unit tensor.

2.2.2 Structural equations

The velocity of the structure $\boldsymbol{v}_s$ is determined by the Cauchy momentum equation that describes the non-relativistic momentum transport in any continuum.

$$\rho_s \frac{D\boldsymbol{v}_s}{Dt} - \nabla.\boldsymbol{\sigma}_s = \rho_s \boldsymbol{f}_s \tag{3}$$

In this equation ρ_s represents the structural density, $\boldsymbol{\sigma}_s$ the Cauchy stress tensor and $\boldsymbol{f}_s$ the body forces per unit of mass on the structure. The notation *D/Dt* refers to the material derivative.

2.2.3 FSI equilibrium conditions

The equilibrium conditions on the fluid-structure interface are the kinematic condition

$$\boldsymbol{v}_f = \boldsymbol{v}_s \tag{4}$$

and the dynamic condition

$$\boldsymbol{\sigma}_f.\boldsymbol{n}_f = -\boldsymbol{\sigma}_s.\boldsymbol{n}_s. \tag{5}$$

$\boldsymbol{n}_f$ and $\boldsymbol{n}_s$ represent the unit normal vector that points outwards from the fluid respectively the structural domain.

2.3 Numerical Model

The fluid domain was meshed using an unstructured grid, as shown in Figure 3, with an initial length of the cell edges of 0.36 mm. This corresponds to a cell density of 15.4 cells/mm^2. The parts attached to the circular cylinder at the in- and outlet of the pump were added to improve the convergence of the iterations in the flow solver. In these parts, the size of the cells increases towards the in- and outlet. If a uniform, fine mesh were used near the in- and outlet, then vortices in the flow near the in- and outlet boundary conditions would cause convergence problems of the flow solver. The Reynolds number of the flow is calculated by considering the membrane as a flat plate, using $r_{s,ext} - r_{s,int}$ and the maximal velocity between the membrane and the casing. As this Reynolds number was approximately 43000 and thus well below the critical Reynolds number for a flat plate, the flow was assumed to be laminar. The flow solver used first-order discretization for the pressure and first-order upwind for the momentum. The time integration scheme was implicit Euler backward. The PISO coupling scheme was used to handle the coupling between pressure and velocity fields. The structural solver used implicit time integration. 160 elements with 8 nodes were used, which corresponds to a cell density of 5.3 cells/mm^2. The geometric nonlinearities due to the large deformation of the structure were taken into account. The fluid and the structure are both considered incompressible. In all computations 200 time steps per cycle were used. All simulations started from the rest state and were carried out until periodicity was achieved. Periodicity is reached when the change of the energy

stored in the fluid domain after 1 period of time is less than 1% of the power needed to induce the membrane motion.

To obtain a high-quality mesh throughout the simulations an innovative combination of mesh motion corresponding to the solution of Laplace equations, mesh smoothing and remeshing is used.

The Laplace equations solved to determine the mesh motion in the entire fluid domain are given by

$$\Delta u_x = 0 \tag{6a}$$

$$\Delta u_y = 0 \tag{6b}$$

with u_x and u_y the displacement of the grid nodes in the x and the y direction respectively. At the fixed boundaries of the domain and at the axis of symmetry u_x and u_y are set to zero. At the fluid-structure interface u_x and u_y are adapted to the interface displacement provided by the coupling code. Afterwards, remeshing and spring-based smoothing, in which the spring stiffness is proportional to the distance between the grid nodes, are applied to the moving grid to improve its quality. Remeshing is performed if the skewness of the cells or the length of the cell edges becomes too large. If the skewness after splitting the cells would be too large, the cells will not be split. This explains the relatively large cells at some locations, as can be seen in Figure 3. Remeshing also limits the minimum length of the cell edges.

2.4 Coupling technique

As mentioned before the fluid-structure interaction is analysed in a partitioned way. The flow solver and structural solver are coupled with the interface quasi-Newton technique with an approximation for the inverse of the Jacobian from a least-squares model (IQN-ILS). In [3] the IQN-ILS technique is compared with other partitioned schemes, such as Aitken relaxation [4] and Interface-GMRES(R) [5]. This comparison indicates that fewer coupling iterations per time step are required if the IQN-ILS algorithm is used. This algorithm influences only the interface displacement, all remaining variables in the fluid and solid domain are considered as internal variables.

The flow solver can be described by following equation

$$\boldsymbol{y} = \mathcal{F}(\boldsymbol{x}) \tag{7}$$

with $\boldsymbol{x}$ the discretized displacement of the fluid-structure interface. This displacement is given to the flow code, which adapts the grid accordingly and then calculates the flow in the entire fluid domain, including the stress distribution $\boldsymbol{y}$ on the interface.

The structural solver is represented by the function

$$\boldsymbol{x} = \mathcal{S}(\boldsymbol{y}) \tag{8}$$

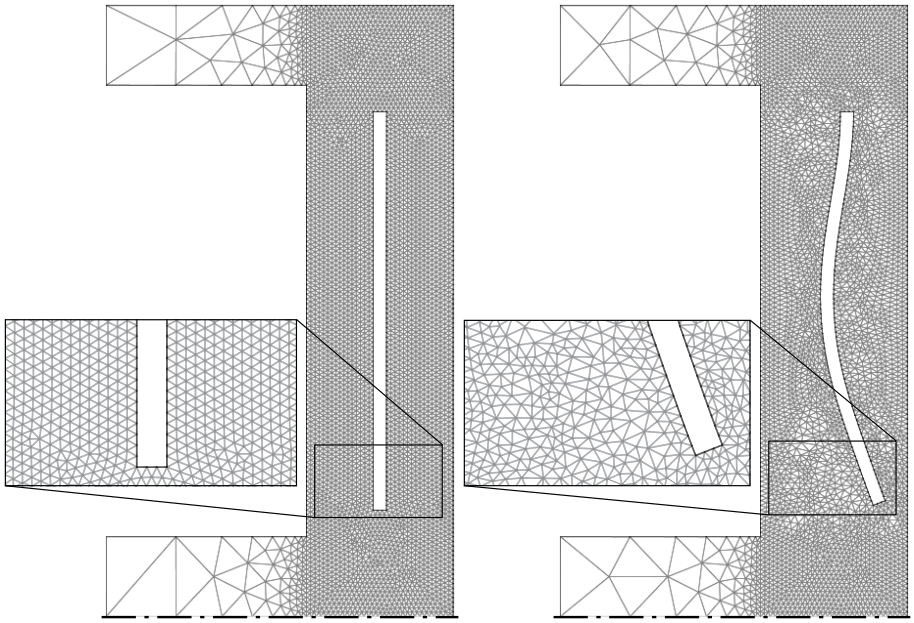

Figure 3: (a) the undeformed grid at the beginning of the calculations and (b) the deformed grid at the moment of maximum deflection obtained with the mesh motion technique described in Section 2.3.

The structural code will calculate the displacement of the structure including the displacement of the fluid-structure interface, based on the stress distribution on the interface.

With these definitions the FSI problem can be formulated as

$$\boldsymbol{x} = \mathcal{S} \circ \mathcal{F}(\boldsymbol{x}) \tag{9}$$

or

$$\mathcal{R}(\boldsymbol{x}) = \mathcal{S} \circ \mathcal{F}(\boldsymbol{x}) - \boldsymbol{x} = 0 \tag{10}$$

with $\mathcal{R}$ the residual operator. In the remainder of this paper, a left superscript indicates the time level; this superscript is omitted if the time level is n+1. A right superscript denotes the coupling iteration.

The FSI problem described by equation (10) can be solved using Newton-Raphson iterations. The equations that have to be solved are given by

$$\left.\frac{d\mathcal{R}}{d\boldsymbol{x}}\right|_{\boldsymbol{x}^k} \Delta\boldsymbol{x}^k = -\boldsymbol{r}^k \tag{11a}$$

$$\boldsymbol{x}^{k+1} = \boldsymbol{x}^k + \Delta\boldsymbol{x}^k \tag{11b}$$

with the residual calculated as

$$\boldsymbol{r}^k = \mathcal{R}(\boldsymbol{x}^k) = \mathcal{S} \circ \mathcal{F}(\boldsymbol{x}^k) - \boldsymbol{x}^k = \tilde{\boldsymbol{x}}^k - \boldsymbol{x}^k \tag{12}$$

The output of the structural solver is indicated with a tilde, as this value is not passed to the next coupling iteration. Convergence of the Newton-Raphson iterations is reached when $||\boldsymbol{r}||_2 \leq \epsilon$ (with ϵ the convergence criterion).

The exact Jacobian of $\mathcal{R}$ is unknown, as we do not know the Jacobians of the black-box solvers $\mathcal{F}$ and $\mathcal{S}$. In [3] and [6] it is shown that only an approximate Jacobian is needed, as long as it describes the reaction to the components of the error on the interface's position that are unstable or disappear slowly in Gauss-Seidel iterations between the flow solver and the structural solver.

Equation (11) can be written as

$$\boldsymbol{x}^{k+1} = \boldsymbol{x}^k + \widehat{\left(\frac{d\mathcal{R}}{d\boldsymbol{x}} \bigg|_{\boldsymbol{x}^k} \right)}^{-1} (-\boldsymbol{r}^k), \tag{13}$$

in which the hat indicates an approximation. The product of the approximation for the inverse of the Jacobian with the vector $-\boldsymbol{r}^k$ will be calculated with data obtained during the previous coupling iterations and optionally with data from previous time steps. The reuse of data from previous time steps can accelerate the convergence if this data is relevant for the current time step.

Two matrices ${}^{n+1}\boldsymbol{V}^k$ and ${}^{n+1}\boldsymbol{W}^k$ are constructed

$${}^{n+1}\boldsymbol{V}^k = [\Delta\boldsymbol{r}^{k-1}\ \Delta\boldsymbol{r}^{k-2}\ \ldots\ \Delta\boldsymbol{r}^1\ \Delta\boldsymbol{r}^0] \tag{14a}$$

$${}^{n+1}\boldsymbol{W}^k = [\Delta\tilde{\boldsymbol{x}}^{k-1}\ \Delta\tilde{\boldsymbol{x}}^{k-2}\ \ldots\ \Delta\tilde{\boldsymbol{x}}^1\ \Delta\tilde{\boldsymbol{x}}^0] \tag{14b}$$

with

$$\Delta\boldsymbol{r}^i = \boldsymbol{r}^{i+1} - \boldsymbol{r}^i \tag{15a}$$

$$\Delta\tilde{\boldsymbol{x}}^i = \tilde{\boldsymbol{x}}^{i+1} - \tilde{\boldsymbol{x}}^i \tag{15b}$$

for i = 0, …, *k*-1. If data from *q* previous time steps is used, the matrices ${}^{n+1}\boldsymbol{V}^k$ and ${}^{n+1}\boldsymbol{W}^k$ are combined with the matrices $\boldsymbol{V}$ and $\boldsymbol{W}$ from previous time steps resulting in

$$\boldsymbol{V}^k = [{}^{n+1}\boldsymbol{V}^k\ {}^{n}\boldsymbol{V}\ \ldots\ {}^{n-q+2}\boldsymbol{V}\ {}^{n-q+1}\boldsymbol{V}] \tag{16a}$$

$$\boldsymbol{W}^k = [{}^{n+1}\boldsymbol{W}^k\ {}^{n}\boldsymbol{W}\ \ldots\ {}^{n-q+2}\boldsymbol{W}\ {}^{n-q+1}\boldsymbol{W}] \tag{16b}$$

The vectors $\Delta \boldsymbol{r} = \boldsymbol{0} - \boldsymbol{r}^k$ and $\Delta \tilde{\boldsymbol{x}} = \tilde{\boldsymbol{x}}^{k+1} - \tilde{\boldsymbol{x}}^k$ are approximated as a linear combination of the known $\Delta \boldsymbol{r}^i$ and $\Delta \tilde{\boldsymbol{x}}^i$

$$\Delta \boldsymbol{r} \approx \boldsymbol{V}^k \boldsymbol{c}^k \tag{17}$$

$$\Delta \tilde{\boldsymbol{x}} = \boldsymbol{W}^k \boldsymbol{c}^k \tag{18}$$

with $\boldsymbol{c}^k$ the coefficients of the decomposition. Considering that the number of columns in $\boldsymbol{V}^k$ is generally much smaller than the number of rows, determined by the number of degrees-of-freedom on the interface, Equation (17) is an overdetermined system with respect to the elements of $\boldsymbol{c}^k$. The least-squares method is applied to solve this linear system. A QR-decomposition of $\boldsymbol{V}^k$ is calculated resulting in the orthogonal matrix $\boldsymbol{Q}^k$ and the upper triangular matrix $\boldsymbol{R}^k$. The coefficients of the decomposition $\boldsymbol{c}^k$ are then calculated by solving the triangular system

$$\boldsymbol{R}^k \boldsymbol{c}^k = {\boldsymbol{Q}^k}^T \Delta \boldsymbol{r}. \tag{19}$$

Considering Equation (12), $\Delta \boldsymbol{r}$ can be written as

$$\Delta \boldsymbol{r} = \Delta \tilde{\boldsymbol{x}} - \Delta \boldsymbol{x}. \tag{20}$$

The approximation for the product of the inverse of the Jacobian with the vector $-\boldsymbol{r}^k$ can thus be calculated as

$$\Delta \boldsymbol{x} = \widehat{\left(\frac{d\mathcal{R}}{d\boldsymbol{x}} \bigg|_{\boldsymbol{x}^k} \right)^{-1}} \Delta \boldsymbol{r} = \boldsymbol{W}^k \boldsymbol{c}^k + \boldsymbol{r}^k. \tag{21}$$

It can be demonstrated that Newton iterations are performed for the part of $\Delta \boldsymbol{r}$ in the span of the columns of $\boldsymbol{V}^k$ and that Gauss-Seidel iterations are performed for the part of $\Delta \boldsymbol{r}$ orthogonal to the span of the columns of $\boldsymbol{V}^k$.

Each time step begins with an extrapolation of the interface's displacement based on the previous time steps. Because data from the previous coupling iterations (and optionally from q previous time steps) is needed to calculate the approximation for the product of the inverse of the Jacobian with the vector $-\boldsymbol{r}^k$, a relaxation with a constant factor $\omega = 10^{-4}$ is performed in the second coupling iteration of the first time step (and in the second iteration of each time step if no data from previous time steps is used).

3 Results

3.1 Mesh and time step refinement

To reduce the computation time, the influence of the mesh and time step refinement on the flow and on the structure deformation are examined separately, without any coupling between the two solvers.

3.1.1 Flow

To determine the number of cells and the number of time steps per cycle required to obtain a time step and grid independent flow field, only the fluid flow was calculated. The displacement of the fluid-structure interface is imposed by a prescribed function, given by

$$x = \pm\frac{t_s}{2} + 0.3 w_{pump} sin(2\pi \frac{r_{pump} - y}{r_{pump} - r_{s,int}} - 2\pi f t) \tag{22}$$

where a plus sign at the beginning of the equation is used for the nodes on the right side of the membrane and a minus sign for the nodes on the left side. x and y represent the x and y coordinate of the interface respectively, t_s the thickness of the structure, w_{pump} the width of the fluid domain, r_{pump} the fluid domain radius, $r_{s,int}$ the internal radius of the structure, t the time and f the excitation frequency. This function implies a sinusoidal traveling wave in the membrane with an amplitude of 0.3 times the width of the fluid domain and a spatial period equal to the length of the radial section.

The same computation for different mesh refinements was performed, keeping the time step size constant at 2x10^{-4} s. The mass flow rate and the stress distribution at the end of the second period are compared with the mass flow rate and the stress distribution obtained with the finest mesh. From Table 2 it can be seen that, if the time step is constant and using a cell density of 15.4 cells/mm^2, the difference in mass flow rate and in maximum pressure is about 1.9% and 5.3%, respectively.

cell density [cells/mm^2]	difference in mass flow rate [%]	difference in maximum pressure [%]
60.3	0	0
26.4	0.67	3.00
15.4	1.90	5.30
11.2	2.97	5.92
6.6	7.27	8.90

Table 2: Influence of the mesh refinement on the difference in mass flow rate and in maximum pressure at the end of the second period.

We repeated the same procedure with a fixed cell density of 17.2 cells/mm^2 and a variable number of time steps per cycle. The results are shown in Table 3. If the mesh size is constant and using 200 time steps per cycle, the difference in mass flow rate and the mean difference in pressure on the left side of the membrane at the end of the second period is about 4.0% and 8.7%, respectively.

3.1.2 Structural deformation

In this section, only the mechanical deformation of the membrane is calculated in the absence of any load on its boundaries. The influence of the mesh size and the number

number of time steps per cycle	difference in mass flow rate [%]	mean difference in pressure [%]
800	0	0
400	0.97	2.07
200	4.01	8.74
100	8.50	17.26
40	17.80	18.27

Table 3: Influence of the number of time steps per period on the difference in mass flow rate and the mean difference in pressure on the left side of the membrane at the end of the second period.

of time steps per period on the maximum deflection of the membrane during the fifth period is examined. The difference between this deflection and the maximum deflection obtained with the finest mesh, respectively obtained with the highest number of time steps per period is calculated. The difference between simulations, using 200 or 400 time steps per period and a cell density of 5.3 or 21.4 cells/mm^2 in the structural domain is negligible (see Table 4 and Table 5).

cell density [cells/mm^2]	difference in maximum deflection [%]
21.4	0
5.3	0.26
1.4	2.31
0.7	4.01

Table 4: Influence of the mesh refinement on the difference in maximum deflection of the membrane during the fifth period.

number of time steps per cycle	difference in maximum deflection [%]
400	0
200	0.08
100	2.30
50	9.78

Table 5: Influence of the number of time steps per period on the difference in maximum deflection of the membrane during the fifth period.

3.2 Fluid-structure interaction

3.2.1 Analysis of the flow field

In Figure 4 a vector plot of the velocity at the moment of maximum deflection is shown. As the simulation is axisymmetric, the flow section decreases from the inlet on the side of the cylinder to the outlet on the axis. As a result, the velocity increases from inlet to outlet.

Periodicity is achieved after approximately 30 periods. The mean mass flow rate is calculated by averaging the instantaneous mass flow rate over one period of excitation in the periodic regime. This instantaneous mass flow rate fluctuates between 89.4 and 100.2 g/s. The mean mass flow rate in the periodic regime is 95.6 g/s. The mean pressure increase across the pump (in- and outlet channels not included) is 19.3 Pa.

3.2.2 Analysis of the deformation of the structure and the stress in the membrane

In Figure 5 the deflection of three points located at three different positions on the membrane is shown during one period of excitation. At an excitation frequency of 50 Hz the radial section of the membrane nearly equals the spatial period of the wave. The deflection of a point near the outer edge of the membrane is approximately in phase with the deflection of a point at the membrane's centre. The deflection of a point halfway the membrane is approximately in antiphase with the deflection of a point at the outer edge.

The maximum deflection of the point halfway the membrane approaches the excitation amplitude. Conversely, the maximum deflection of the point at the membrane's centre is approximately a factor of 3 higher than the excitation amplitude. This relatively large displacement restricts the excitation amplitude, because the membrane should stay within the limits of the fluid domain. Hence, the distance between the membrane and the pump casing is quite large, except near the centre of the pump. This entails a large backflow.

We remark that, although a sinusoidal motion is applied to the outer edge of the membrane, the deflections of all other points are asymmetrical. This is due to the geometry of the pump (the parts at the in- and outlet), which is not symmetrical with respect to the membrane plane at rest.

In Figure 6 the components of the stress $\sigma_{xx},\ \sigma_{yy},\ \sigma_{xy}$ and σ_{zz} are shown at the moment of maximum deflection. The σ_{zz} stress component reaches the highest values. This occurs at the centre of the membrane. It is clear that the central opening enlarges with the slightest membrane motion.

3.2.3 Energetic analysis of the pump

First, a power study is performed considering the structural domain as the control volume. The power entering the control volume is the excitation power, required to

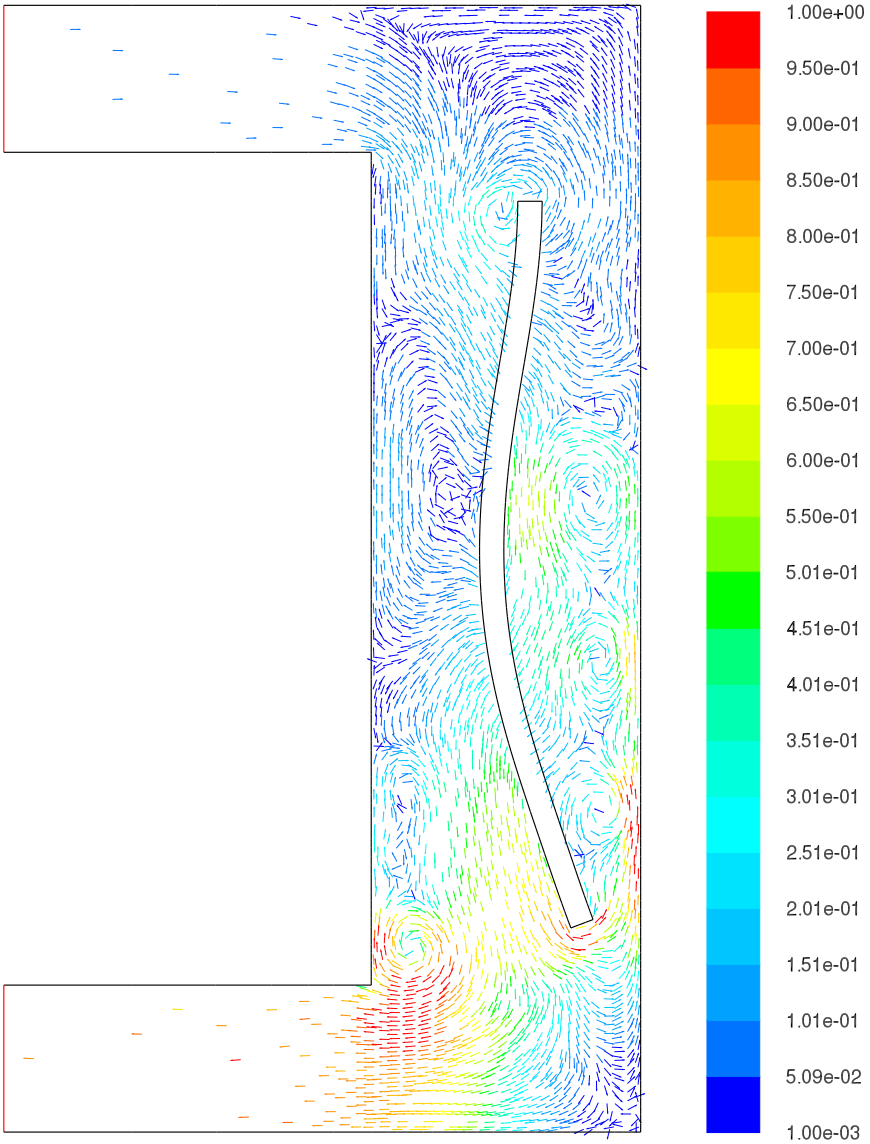

Figure 4: Vector plot of the velocity at the moment of maximum deflection.

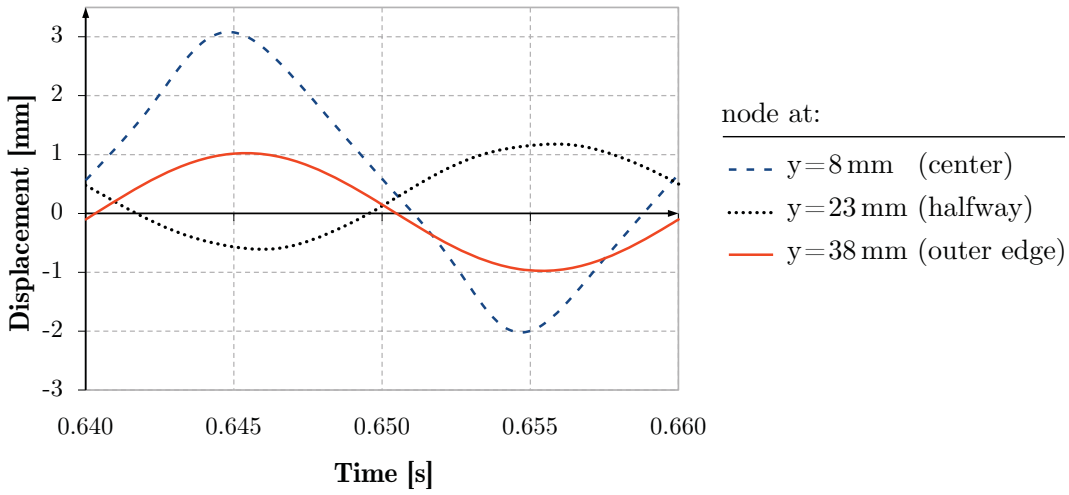

Figure 5: Evolution of the deflection in the axial direction of a point located at the membrane's centre, halfway the membrane and at the outer edge of the membrane.

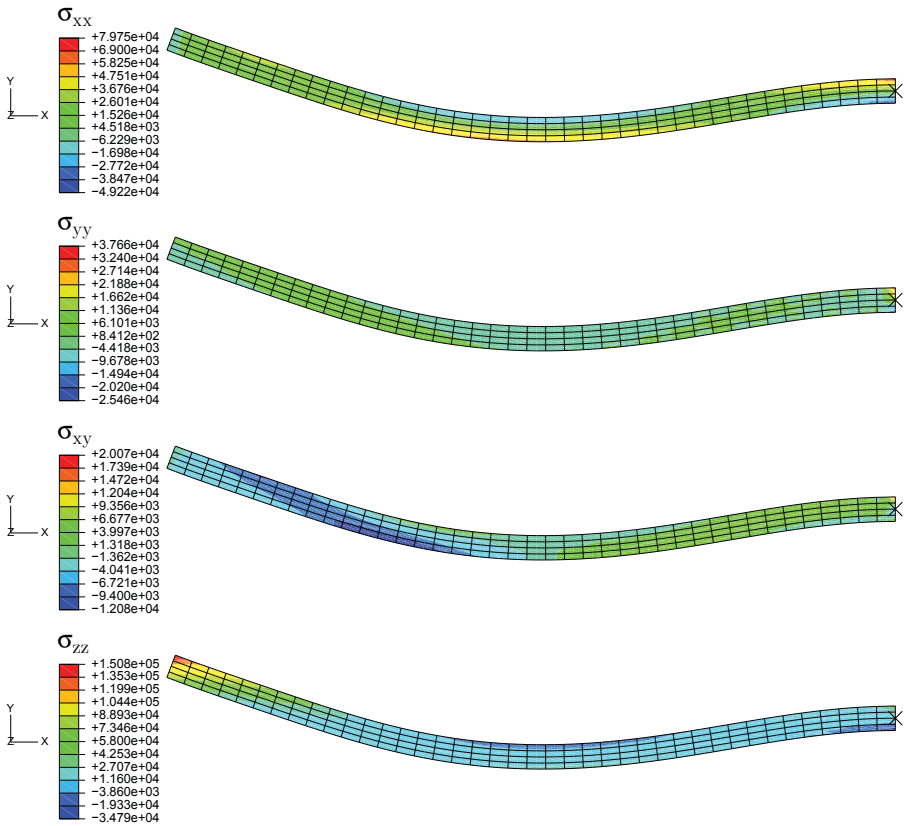

Figure 6: Contour plot of the components of the stress σ_{xx}, σ_{yy}, σ_{xy} and σ_{zz} at the moment of maximum deflection.

move the structure. This power is calculated as

$$P_{excitation} = \boldsymbol{f}_r.\boldsymbol{v}_r \tag{23}$$

with $\boldsymbol{f}_r$ the driving force exercised on the membrane and $\boldsymbol{v}_r$ the velocity of the outer edge of the membrane. The power leaving the control volume is the power transferred to the fluid through the membrane. This power is determined by

$$P_{membrane\ to\ fluid} = \iint (\boldsymbol{\sigma n}).\boldsymbol{v} dS \tag{24}$$

where the integral is taken over the entire surface of the membrane, $\boldsymbol{\sigma}$ represents the stress tensor on the membrane surface, $\boldsymbol{n}$ the unit normal vector pointing out the structural domain and $\boldsymbol{v}$ the membrane velocity. Although the powers (23) and (24) differ instantaneously, their time average over one period should be equal because no energy is dissipated in the structure. The difference between both powers is given by the change in energy stored in the membrane per unit of time. This energy consists of two parts: the kinetic energy and the strain energy. The maximum strain energy is reached when the deflection of the membrane is maximal; at that time the kinetic energy reaches its minimum. In Figure 7 the evolution is shown of the excitation power, the change in total energy stored in the membrane per unit of time (both calculated by the structural solver) and the power transferred to the fluid through the membrane during one period of excitation (calculated by the flow solver). It can be seen that although a different grid size had been used to mesh the fluid and structural domain, the power transferred to the fluid through the membrane computed by the structural solver, i.e. the difference between the excitation power and the change in energy stored in the membrane per unit of time, is a very good approximation of the power transferred to the fluid calculated by the flow solver. The mean excitation power (0.1283 W) in one period nearly equals the mean power transferred to the fluid (0.1282 W). The small difference between both values is due to the fact that the motion of the structure is not perfectly periodic after 32 periods such that the total energy stored in the structure still changes slightly (0.0001 W).

Secondly, a power study is performed considering the fluid domain as the control volume. The power transferred to the fluid through the surface of the membrane is now the incoming power. The power leaving the control volume consists of two parts: a useful part, i.e. pump power, and the dissipated power. The equations used to calculate these powers are given by

$$P_{pump} = \dot{V}(p_{tot,out} - p_{tot,in}) \tag{25}$$

$$P_{dissipated} = \dot{m} c_p (T_{out} - T_{in}) \tag{26}$$

with $\dot{V}$ the volume flow rate, $p_{tot,in}$ and $p_{tot,out}$ the mass weighted average total pressure at in- and outlet, $\dot{m}$ the mass flow rate and T_{in} and T_{out} the mass weighted average temperature at in- en outlet. The difference between the incoming and the outgoing power is given by the change in energy stored in the fluid domain per unit of time.

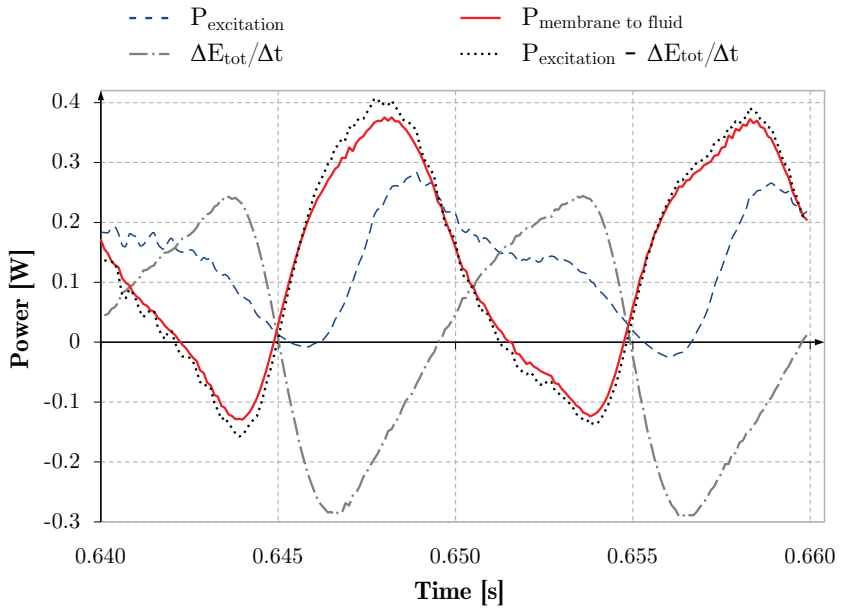

Figure 7: Evolution of the excitation power, the change in energy stored in the membrane per unit of time and the power transferred to the fluid through the membrane during one period of excitation.

The energy stored in the fluid domain is the sum of the kinetic energy and the internal energy of the fluid present in the pump. The change in total energy E per unit of time is calculated as

$$\frac{dE}{dt} = \rho_f \frac{1}{2} \iiint \frac{dv^2}{dt} dV + \rho_f c_v \iiint \frac{dT}{dt} dV \tag{27}$$

where the integrals are taken over the entire fluid domain. In Figure 8 the evolution of the powers calculated with Equations (25), (26) and (27) is shown during one period of excitation. The mean pump power is 0.0217 W. The mean dissipated power is 0.1060 W, which corresponds to a temperature rise of 0.000267 K. The mean change in total energy per unit of time is 0.000013 W, a very small value, which indicates the flow is nearly periodic.

The efficiency of the pump is defined as

$$\eta = \frac{P_{pump}}{P_{excitation}} \tag{28}$$

where the pump power and the excitation power are calculated using Equations (25) and (23), respectively. Because the parts at the in- and outlet are not parts of the pump itself, the mass weighted average total pressures in Equation (25) are taken at the end of the inlet section and at the beginning of the outlet section. The mean pump power calculated this way is 0.0388 W. With a mean excitation power of 0.1283 W an efficiency of 30.3% is obtained. This relatively low value is due to the relatively large

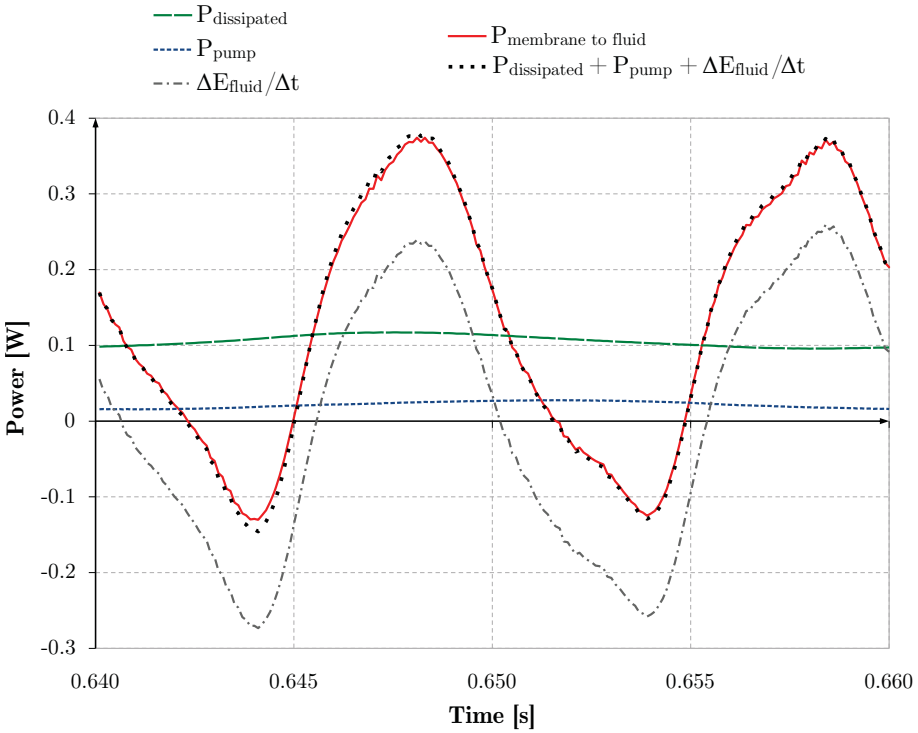

Figure 8: Evolution of the power transferred to the fluid through the membrane, the dissipated power, the pump power, the change in energy stored in the fluid domain per unit of time and the sum of these last three powers during one period of excitation.

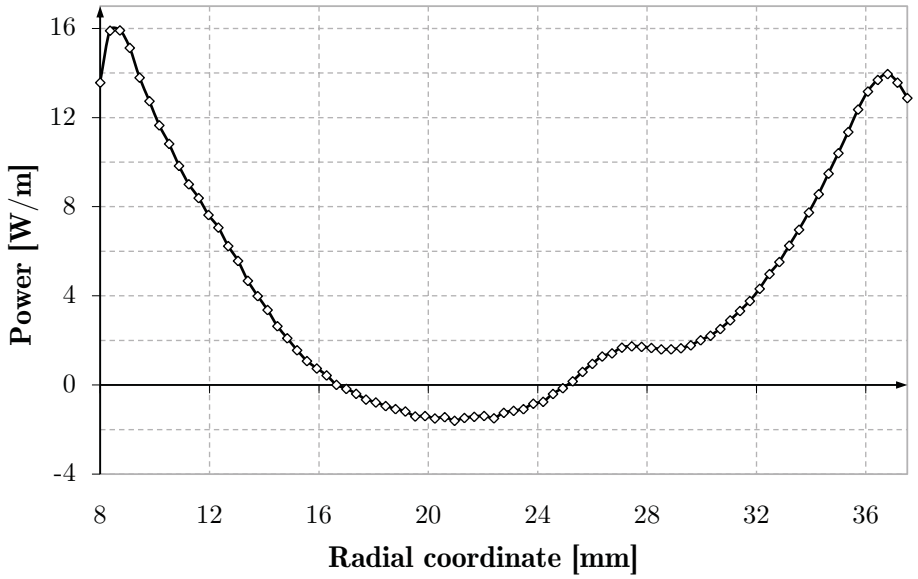

Figure 9: Distribution of the mean power transferred from the membrane to the fluid through the fluid-structure interface, averaged over one period.

distance between the pump casing and the membrane that entails a large backflow. However, for biomedical applications, efficiency is not the primary concern.

In Figure 9 the distribution of the mean power transferred to the fluid at each node along the fluid-structure interface is shown averaged over one period. This shows that most of the energy is transferred near the central opening of the membrane and near the outer edge where the excitation is performed. Halfway the membrane work is done by the fluid on the membrane.

4 Conclusions

The simulation of the fluid-structure interaction in the membrane pump is been made possible by using the IQN-ILS coupling technique and by using a combination of mesh motion corresponding to the solution of Laplace equations, mesh smoothing and remeshing. The mean mass flow rate supplied by the pump is 95.6 g/s. The deflection of a point at the membrane's centre is approximately a factor of 3 higher than the excitation amplitude. This large displacement restricts the excitation amplitude. The relatively large distance between the membrane and the casing of the pump entails a large backflow which consequently leads to a relatively low pumping efficiency of about 30%. Although a different grid size has been used to mesh the fluid and structural domain, the power transferred to the fluid through the membrane calculated with the structural solver, equals the power transferred to the fluid calculated with the flow solver.

References

[1] A. S. Forouhar, M. Liebling, A. Hickerson, A. Moghaddam, H.-J. Tsai, J. R. Hove, S. E. Fraser, M. E. Dickinson, and M. Gharib, "The embryonic vertebrate heart tube is a dynamic suction pump", Science, 312, 751, 2006.

[2] L. Loumes, I. Avrahami, and M. Gharib, "Resonant pumping in a multilayer impedande pump", Physics of Fluids, 20, 2008.

[3] J. Degroote, K.-J. Bathe, and J. Vierendeels, "Performance of a new partitioned procedure versus a monolithic procedure in fluid-structure interaction", Computers and Structures, 87(11-12), 793-801, 2009.

[4] U. Küttler and W. Wall, "Fixed-point fluid-structure interaction solvers with dynamic relaxation", Computational Mechanics, 43(1), 6172, 2008.

[5] C. Michler, E.H. van Brummelen, R. de Borst, "An interface Newton-Krylov solver for fluid-structure interaction", International Journal for Numerical Methods in Fluids, 47(10-11), 1189-1195, 2005.

[6] J. Degroote, P. Bruggeman, R. Haelterman and J. Vierendeels, "Stability of a coupling technique for partitioned solvers in FSI applications", Computers and Structures, 86(23-24), 2224-2234, 2008.